Supplemental Material for: Spatio-temporal patterns in ultra-slow domain wall creep dynamics

Ezequiel E. Ferrero, Laura Foini, Thierry Giamarchi, Alejandro B. Kolton, and Alberto Rosso

In this supplement we describe in details our model and validate it. We confirm that creep motion is described by both depinning and equilibrium exponents by inspecting the Random Field disorder case in comparison with the Random Bond used along the main text. Finally, we provide quantitative estimates of the relevant scales for the experimental test of our results in Pt/Co/Pt thin ferromagnetic films.
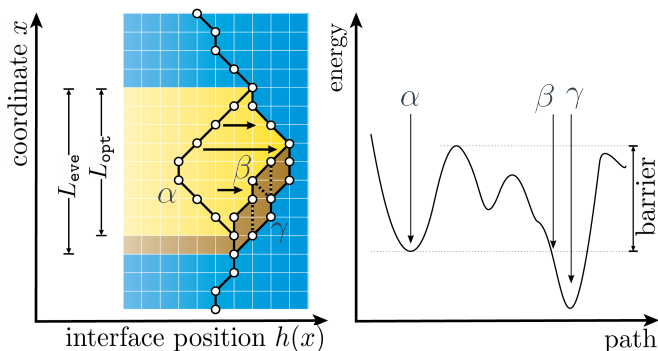
FIG. S1. *The 2-step creep algorithm* – On the left, a schematic representation of the interface moving from a blocked configuration α to a new one γ, passing trough the intermediate unstable configuration β. An activated nucleus of size L_{opt} takes the system from α to β. From there, a sequence of deterministic VMC relaxation updates follows, represented by dashed lines, leaving the system in a new metastable state that differs from the previous one in a portion L_{eve}. On the right, a simplified energy-path draw that illustrates this action.

MODEL DETAILS

The interface is modeled as a discrete polymer of L monomers at integer positions $h(i)$ ($i = 0, \ldots, L - 1$). The string energy is given by:

$$E = \sum_i \left[(h(i+1) - h(i))^2 - fh(i) + V(i, h(i)) \right]. \quad \text{(S1)}$$

We consider periodic boundary conditions in the longitudinal direction ($h(L) \equiv h(0)$), and implement a hard metric constraint ($|h(i) - h(i-1)| \leq 1$) which significantly reduces the configuration space [1]. The disorder $V(h(i), i)$ is computed from uncorrelated Gaussian numbers $R_{j,i}$ with zero mean and unit variance. To model RB disorder we defined $V_{RB}(h, i) = R_{h,i}$, such that $\overline{V(j,i)V(j',i')} = \delta_{i,i'}\delta_{j,j'}$ while for RF disorder we define $V_{RF}(h, i) = \sum_{k=0}^{h} R_{k,i}$, such that $\overline{[V_{RF}(j,i) - V_{RF}(j',i')]^2} = \delta_{i,i'}|j - j'|$.

The two-steps polymer position update, illustrated in Fig. S1, is performed as follows:

(i) Activation: Starting from any metastable state we find the smallest compact rearrangement that decreases the energy. In order to do that, we fix a window w and compute the optimal path between two generic points $i, i + w$ of the polymer using the Dijktra's algorithm adapted to compute the minimal energy polymer between two fixed points [2] (we do it for all i). The minimal favorable rearrangement corresponds to the minimal window, w, for which the best path differs from the polymer configuration. In practice, the window w is increased from $w = 2$ up to the minimal $w_{\min}$ needed to decrease the energy of the polymer. If in correspondence with $w_{\min}$ multiple possible rearrangements are found (namely multiple choice of the starting point i), we select the one which triggers the polymer to the smallest energy. Within this approach, as discussed in the main article, we assume that the minimal energy barrier identifies with the smallest compact movement that decreases the energy.

(ii) Deterministic relaxation: After the above activated move, the string is not necessarily in a new metastable state. So, we let the line relax deterministically with a protocol of elementary moves [3] also known as Variant Monte Carlo (VMC) [4], which allows for the motion of $m + 1$ adjacent sites by one lattice spacing if no move of m sites is energetically favorable.

We are interested in a steady state behavior. One could define the onset of a stationary state as the configuration in which two different initial conditions start to visit exactly the same sequence of metastable states. We have explicitly checked, stating from different flat initial states, that this is established after each point of the line has advanced forward at least a small portion of its length, and we use that as a criterion to discard the transient.

The approximation introduced in the activated step allowed us to overcome the severe computation limitations of the exact algorithm and made it possible not only to increase by a factor 30 the system size, but, and more importantly, to decrease by a factor 100 the external drive f, unveiling the statistics and the clustering of the activated events. Indeed, as discussed in [2, 5], the computational cost of the activated step grows exponentially in $L_{\text{opt}}(f)$ with the exact algorithm while, within our approximation, it has a polynomial cost. Of course, there is a price to pay: We lose access to the actual energy barrier values and therefore to the real time. On top of the algorithmic improvement, the ensemble of our
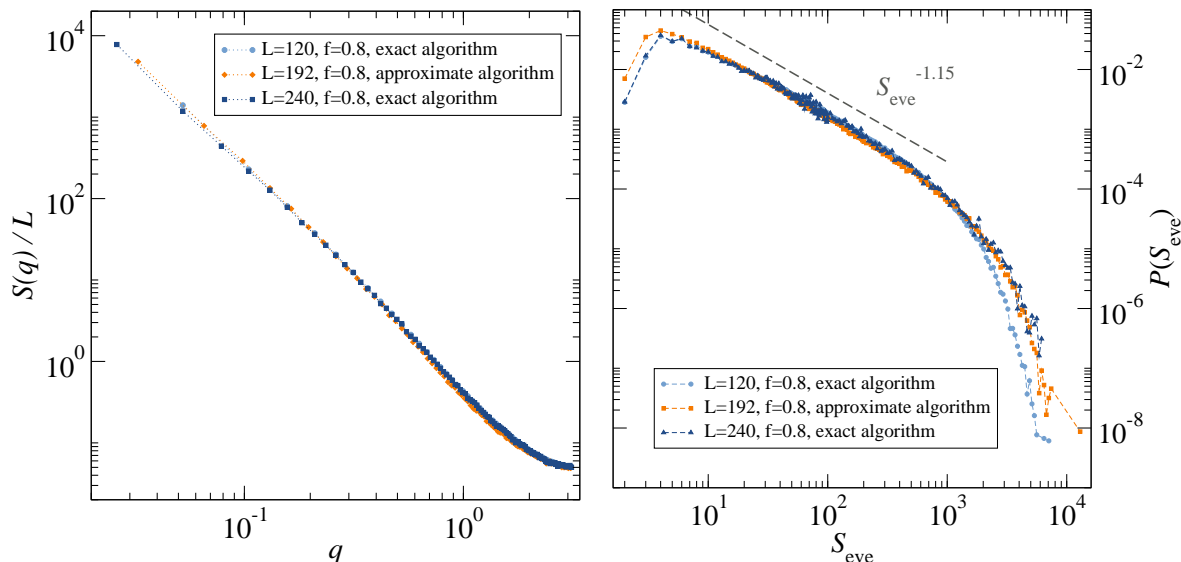
FIG. S2. *Left:* Average structure factors in the steady-state creep motion at $f = 0.8$. We compare the structure factor obtained with the approximate algorithm for $L = 192$, with the ones obtained with the exact algorithm for $L = 120, 240$. *Right:* Comparison of the creep event size distribution obtained with the exact and approximate algorithms for a driving force $f = 0.8$. The power law $P(S_{\mathrm{eve}}) \sim S_{\mathrm{eve}}^{-1.15}$ is shown as a guide to the eye.

code is implemented to run in parallel in general-purpose Graphics Processing Units, what gives an extra speedup to the simulations. Source files are freely available under request.

In order to validate our approximation, we contrast its results directly with the ones obtained by the exact transition pathways algorithm used in Refs. [2, 5]. In Fig.S2-left and S2-right we compare, respectively, the average structure factor and the event size distribution at a given force. A statistical difference can only be appreciated for small events (small length scales and large wave-vectors q), presumably because of disregarding the existence of large energy barriers for some of the small rearrangements. In general the equivalence between the scaling of rearrangement sizes and energy barriers seems to work very well all across the range of parameters where it is possible to simulate both algorithms. Most importantly, differences at large scales, the ones that dominate the universal behavior we aim to study, are unobservable.

RANDOM BOND AND RANDOM FIELD DISORDER

Being an intermediate regime between two fixed points of the dynamics [6], the creep is thus described by both equilibrium and depinning exponents, rather than by different ones.

In Table S1 we report the equilibrium and depinning exponents [2, 5, 7–12] for RB and RF. It is worth remarking that RB and RF share the same depinning universality class while at equilibrium they display different

1d RB exponents	estimate
ζ_{eq}	2/3
$\nu_{\mathrm{eq}} = 1/(2 - \zeta_{\mathrm{eq}})$	3/4
$\tau_{\mathrm{eq}} = 2 - 2/(1 + \zeta_{\mathrm{eq}})$	4/5
$\theta_{\mathrm{eq}} = 2\zeta_{\mathrm{eq}} - 1$	1/3
$\mu = \theta_{\mathrm{eq}}\nu_{\mathrm{eq}}$	1/4
1d RF exponents	**estimate**
$\zeta_{\mathrm{eq}}^{\mathrm{RF}}$	1
$\nu_{\mathrm{eq}}^{\mathrm{RF}} = 1/(2 - \zeta_{\mathrm{eq}}^{\mathrm{RF}})$	1
$\tau_{\mathrm{eq}}^{\mathrm{RF}} = 2 - 2/(1 + \zeta_{\mathrm{eq}}^{\mathrm{RF}})$	1
$\theta_{\mathrm{eq}}^{RF} = 2\zeta_{\mathrm{eq}}^{\mathrm{RF}} - 1$	1
$\mu^{\mathrm{RF}} = \theta_{\mathrm{eq}}^{\mathrm{RF}}\nu_{\mathrm{eq}}^{\mathrm{RF}}$	1
1d RB & RF exponents	**estimate**
ζ_{dep}	1.250
$\nu_{\mathrm{dep}} = 1/(2 - \zeta_{\mathrm{dep}})$	1.333
$\tau_{\mathrm{dep}} = 2 - 2/(1 + \zeta_{\mathrm{dep}})$	1.11

TABLE S1. Universal exponents relevant for the one dimensional creep motion, for short range elastic interactions, according to the disorder type.

exponents.

The fact that RB and RF disorders have the same depinning but different equilibrium exponents has visible consequences in the creep event size distributions. In fact, as can be seen in Fig. S4-left, and comparing with Fig. 3, individual events decays faster for RF than for RB disorder. On the other hand in Fig. S4-right we show that the distribution of cluster sizes decays, for large sizes, as
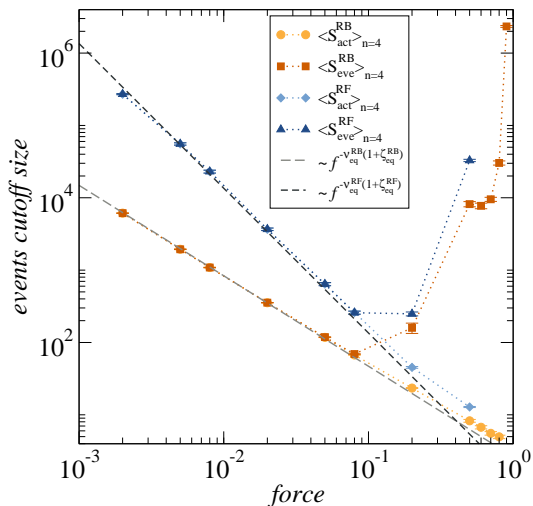
FIG. S3. Cutoff of the distribution of the areas of creep events for RB and RF disorders. In each case the mean value of fourth order $\langle X \rangle_{n=4} = \langle X^4 \rangle / \langle X^3 \rangle$ is shown. The error bars are estimated from the difference with the values given by $\langle X \rangle_{n=3}$. Dashed lines show the universal power-law divergence expected as $f \to 0$ from the phenomenological creep theory, being the $L_{\mathrm{opt}} \sim f^{-\nu_{\mathrm{eq}}}$ law verified for forces $f < 0.1$. Note that $S_{\mathrm{eve}} \approx S_{\mathrm{act}} \sim S_{\mathrm{opt}} = L_{\mathrm{opt}}^{1+\zeta}$ at low forces, while at higher values $S_{\mathrm{eve}} \gg S_{\mathrm{opt}}$ due to large deterministic relaxation. In particular one observes $S_{\mathrm{act}} \sim S_{\mathrm{opt}} \to \infty$ for $f \to 0$ and $S_{\mathrm{eve}} \to \infty$ for $f \to f_c^-$. Data correspond to simulations of a system size $L = 3360$.

a power law with an exponent $\tau_{\mathrm{dep}} \approx 2 - 2/(1 + \zeta_{\mathrm{dep}}) \approx 1.11$, in accordance with Fig. 4 and the fact that depinning exponents are identical for RB and RF. For sizes smaller that S_{opt} however, the RF cluster distribution in Fig. S4-right is better described by a power law decay with exponent $\tau_{\mathrm{eq}}^{\mathrm{RF}} \approx 2 - 2/(1 + \zeta_{\mathrm{eq}}^{\mathrm{RF}}) \approx 1$, which is visually distinguishable from the exponent $\tau_{\mathrm{eq}} \approx 4/5$ of the RB case in Fig.4. As for the case of RB disorder, the structure factor $S(q)$ also accompanies this length crossover, showing a geometrical change at wave-vector $q_c \simeq 1/L_{\mathrm{opt}}(f)$, as displayed in the inset of Fig. S4-right. But notice now that $L_{\mathrm{opt}}(f) \sim f^{-\nu_{\mathrm{eq}}^{\mathrm{RF}}}$, with a different exponent. Consistently, the geometrical crossover is now from the unique depinning roughness ζ_{dep} at large scales, to the RF equilibrium roughness $\zeta_{\mathrm{eq}}^{\mathrm{RF}}$ at small ones.

The good collapse of the curves in Fig. S4-left under the rescaling $S_{\mathrm{eve}}/f^{-\nu_{\mathrm{eq}}^{\mathrm{RF}}(1+\zeta_{\mathrm{eq}}^{\mathrm{RF}})}$ shows that $f^{-\nu_{\mathrm{eq}}^{\mathrm{RF}}(1+\zeta_{\mathrm{eq}}^{\mathrm{RF}})}$ controls the cutoff of the distribution, as it was shown for the RB case in the article. Another way to systematically access the cutoff S_c of a distribution of the form (5) is to look at the higher moments $S_c \approx S_n \equiv \langle S^n \rangle / \langle S^{n-1} \rangle$ with $n > \tau$.

In Fig. S3 we show this ratio for $n = 4$ both for RB and RF. Further, for each type of disorder we show the value obtained considering only the activated part S_{act} of the event (recall the algorithm description above) and

the total area of the event S_{eve} (which is the activated plus the deterministic part). As can be seen comparing with the dashed lines representing $S_{\mathrm{opt}} \sim f^{-\nu_{\mathrm{eq}}(1+\zeta_{\mathrm{eq}})}$ (compatible with the celebrated $L_{\mathrm{opt}} \sim f^{-\nu_{\mathrm{eq}}}$), at small forces one recovers the creep scaling for the high order moment (equivalently, for the cutoff of the distribution) $S_n \sim f^{-\nu_{\mathrm{eq}}(1+\zeta_{\mathrm{eq}})}$, be it RB or RF. At large forces, S_{act} and the total area S_{eve} are significantly different due to the divergence of the deterministic relaxation after activation as we approach f_c, estimated to be $f_c \approx 1.1$ for RB and $f_c \approx 0.9$ for RF in the natural units of our problem.

In fact, S_{eve} is defined as a combination of an activated move of size S_{act}, which diverges for $f \to 0$, plus a deterministic relaxation diverging at $f \to f_c$. Therefore, S_{eve} diverges at both critical points while taking a minimal value at intermediate forces. This, translated to L_{eve}, accompanies the non-monotonic behavior of the MSD discussed before.

In summary, the observations made in this section further confirm that creep motion is generically described by both equilibrium and depinning exponents regardless of the RB or RF nature of the disorder.

QUANTITATIVE ESTIMATIONS FOR THE CASE OF Pt/Co/Pt THIN FILMS

We believe that the clustering of creep events can be observed in experiments with the current apparatus and magneto-optical techniques which are able to directly visualize the interface motion. Indeed, using this technique, Repain et al. [13] already observed, in a He-ion–irradiated Pt/Co(0.5 nm)/Pt ultrathin film, small correlated events in the creep regime whose characteristic size increased with lowering the field, in good qualitative agreement with our predictions. More Recently, Gorchon et al. [14] studied field-driven one dimensional domain walls in ultrathin Pt(0.35nm)/Co(0.45nm)/Pt(0.35nm) magnetic films with perpendicular anisotropy, using magneto-optical Kerr microscopy. By fitting the velocity force characteristics in the creep and depinning regimes, they determined a critical depinning field $H_{\mathrm{dep}} \approx 1000$ Oe and a characteristic energy scale $k_B T_{dep} \approx 2000$ K at room temperature ($T = 300$ K). With these values it is possible to evaluate the linear size of the event cut-off, L_{opt} and the associated displacement, h_{opt}, using the standard assumptions of weak pinning [15–17]:

$$L_{\mathrm{opt}} = L_c(H_{dep}/H)^{\nu_{\mathrm{eq}}} \approx 40nm(H_{dep}/H)^{0.75}, \quad \text{(S2)}$$

$$h_{\mathrm{opt}} = w_c(L_{\mathrm{opt}}/L_c)^{\zeta_{\mathrm{eq}}} \approx 20nm(H_{dep}/H)^{0.5}. \quad \text{(S3)}$$

Here we used the known values for the 1d ν_{eq} and ζ_{eq}, from Table S1. The microscopic length L_c, named Larkin length, can be evaluated [15, 16] as $L_c = (k_B T_{dep})/[(M_s H_{dep}\delta)w_c] \approx 40$ nm, where $w_c \approx 20$ nm is of the order of the domain wall width, $\delta \approx 0.45$ nm
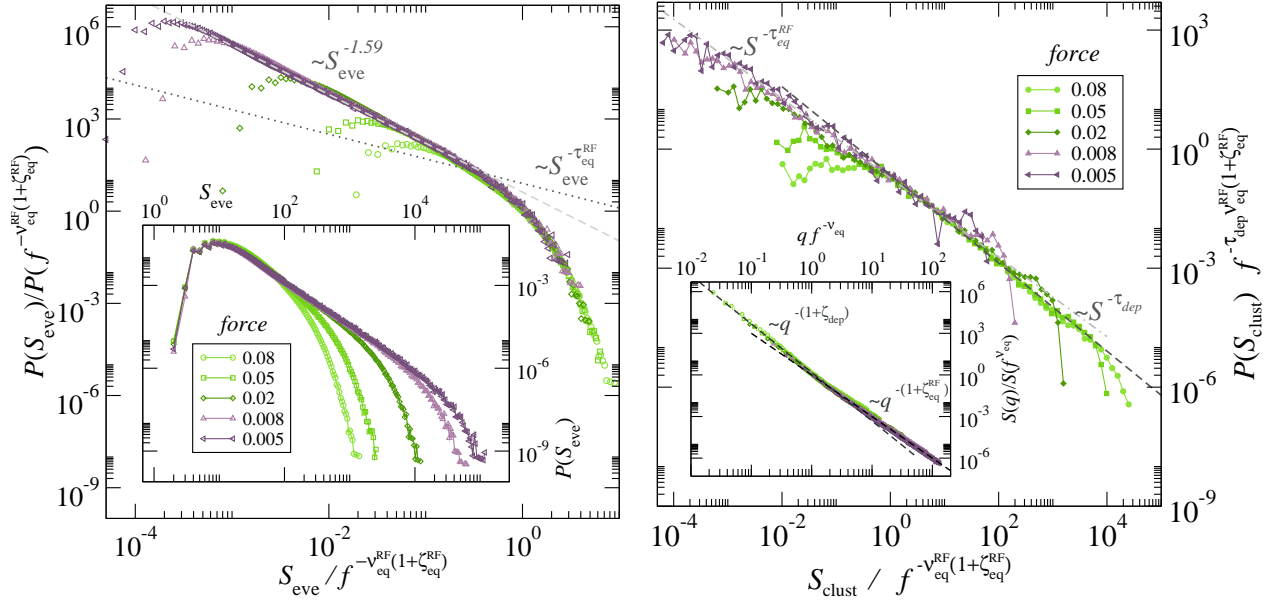
FIG. S4. *Event and cluster size distributions for the Random Field disorder case* – On the left: Distribution of creep events in presence of RF disorder for different forces. The inset shows the $P(S_{\text{eve}})$ as a function of S_{eve} while the main panel shows the collapse obtained using the rescaled variables $P(S_{\text{eve}})/P(f^{-\nu_{\text{eq}}^{\text{RF}}(1+\zeta_{\text{eq}}^{\text{RF}})})$ and $S_{\text{eve}}/f^{-\nu_{\text{eq}}^{\text{RF}}(1+\zeta_{\text{eq}}^{\text{RF}})}$. The collapse confirms the creep scaling for the cutoff $S_c \sim L_{\text{opt}}^{1+\zeta_{\text{eq}}^{\text{RF}}} \sim f^{-\nu_{\text{eq}}^{\text{RF}}(1+\zeta_{\text{eq}}^{\text{RF}})}$. On the right: Cluster size distribution for RF disorder and different forces. As in the RB case a crossover from equilibrium to depinning is observed when we scale S_{clust} with $S_{\text{opt}} \simeq f^{-\nu_{\text{eq}}^{\text{RF}}(1+\zeta_{\text{eq}}^{\text{RF}})}$. Notice that both the scaling size S_{opt} and the exponent of the equilibrium power-law regime ($\tau_{\text{eq}}^{RF} = 1$) have changed respect to the ones of the RB case and still the scaling holds. Data correspond to a system of size $L = 3360$.

is the thickness of the sample and $M_s \approx 800 \ erg/G.cm^3$ the saturation magnetization. Interestingly this implies that the two dimensional shape of creep events become increasingly compressed in the direction of motion as we reduce H, the aspect ratio scaling as $L_{\text{opt}}/h_{\text{opt}} \approx 2(H_{dep}/H)^{0.25}$ (very thin and elongated avalanches). On the other hand, the area distribution cut-off of these events is predicted to scale as

$$S_{\text{opt}} = w_c L_c (L_{\text{opt}}/L_c)^{\zeta_{\text{eq}}+1} \approx 800 \ nm^2 (H_{dep}/H)^{1.25}$$
(S4)

For a given field, detecting individual creep events of such sizes is mainly limited by the spatial resolution of the imaging technique. Using a spatial resolution of $1 \ \mu m$, which is typical for magneto-optical setups, plugging in the measured $H_{dep} \approx 1000 \ Oe$ and asking for $L_{\text{opt}}, h_{\text{opt}} > 1 \ \mu m$, we get the condition $H \lesssim 0.4 \ Oe$ at room temperature. For such fields, $S_{\text{opt}} = h_{\text{opt}} \times L_{\text{opt}} \lesssim 40 \ \mu m \times 1 \ \mu m = 40 \ \mu m^2$ and the average domain wall velocity drops below $1nm/s$, as is found by extrapolating from the creep law. At such small velocities, which are in principle still measurable (e.g. $v_{min} = 0.1 \ nm/s$ in [18]), the "granularity" of creep events should become observable, opening the possibility to test our predictions of spatio-temporal correlations and non-trivial distributions for them.

It is worth mentioning that L_{opt} was also estimated independently in Ta(5.0-nm)/Pt(2.5-nm)/Co90Fe10 (0.3-nm)/Pt(1.0-nm) film wires with perpendicular magnetic anisotropy [19], with a completely different method. Once more, L_{opt} was shown to scale as predicted for the RB 1d model with short-range elasticity $L_{\text{opt}} \sim H^{-0.75}$. This was achieved by observing the onset of finite effects in the velocity force characteristics at the creep regime, as the wire width w was physically reduced down to $w \sim L_{\text{opt}}(H)$ and below. For these samples a field of $H = 16 \ Oe$ gives $L_{\text{opt}} \approx 0.16 \ \mu m$, remarkably in good agreement with the above estimate for the $Pt/Co/Pt$ film. Interestingly enough, our results imply that at low fields, such that $L_{\text{opt}} > w$, the velocity is controlled by a power law distribution of thermally activated events with a size cut-off w. This is consistent with the results reported in [19] showing the scaling of the velocity with w in place of L_{opt}. Moreover, our findings also predict that the so-called "zero dimensional" regime in [19] has actually contributions from power-law distributed correlated events with a size smaller than w.

MOVIE

Accompanying this manuscript we provide a movie illustrating the spatio-temporal patterns in ultra slow creep dynamics as obtained directly from our simulations for a small $L = 512$ system. The movie displays the se-

quence of creep events in space and the corresponding activity maps comparing with depinning avalanches.

————————

[1] This constraint also induces an harmonic-anharmonic depinning crossover at large enough scales, that we consider together with finite size effects in [20].

[2] A. B. Kolton, A. Rosso, T. Giamarchi, and W. Krauth, Phys. Rev. B **79**, 184207 (2009).

[3] A. Rosso and W. Krauth, Phys. Rev. B **65**, 012202 (2001).

[4] A. Rosso and W. Krauth, Computer Physics Communications **169**, 188 (2005), proceedings of the Europhysics Conference on Computational Physics 2004.

[5] A. B. Kolton, A. Rosso, T. Giamarchi, and W. Krauth, Phys. Rev. Lett. **97**, 057001 (2006).

[6] P. Chauve, T. Giamarchi, and P. Le Doussal, Europhys. Lett. **44**, 110 (1998).

[7] M. Kardar, Phys. Rev. Lett. **55**, 2923 (1985).

[8] D. S. Fisher, Phys. Rev. Lett. **56**, 1964 (1986).

[9] O. Narayan and D. S. Fisher, Phys. Rev. B **48**, 7030 (1993).

[10] P. Chauve, P. Le Doussal, and K. Jörg Wiese, Phys. Rev. Lett. **86**, 1785 (2001).

[11] A. Rosso, A. K. Hartmann, and W. Krauth, Phys. Rev. E **67**, 021602 (2003).

[12] E. E. Ferrero, S. Bustingorry, and A. B. Kolton, Phys. Rev. E **87**, 032122 (2013).

[13] V. Repain, M. Bauer, J.-P. Jamet, J. Ferré, A. Mougin, C. Chappert, and H. Bernas, Europhys. Lett. **68**, 460 (2004).

[14] J. Gorchon, S. Bustingorry, J. Ferré, V. Jeudy, A. Kolton, and T. Giamarchi, Phys. Rev. Lett. **113**, 027205 (2014).

[15] A. Larkin and Y. N. Ovchinnikov, Journal of Low Temperature Physics **34**, 409 (1979).

[16] T. Nattermann, Y. Shapir, and I. Vilfan, Physical Review B **42**, 8577 (1990).

[17] V. Démery, A. Rosso, and L. Ponson, EPL (Europhysics Letters) **105**, 34003 (2014).

[18] P. Metaxas, J. Jamet, A. Mougin, M. Cormier, J. Ferré, V. Baltz, B. Rodmacq, B. Dieny, and R. Stamps, Phys. Rev. Lett. **99**, 217208 (2007).

[19] K.-J. Kim, J.-C. Lee, S.-M. Ahn, K.-S. Lee, C.-W. Lee, Y. J. Cho, S. Seo, K.-H. Shin, S.-B. Choe, and H.-W. Lee, Nature **458**, 740 (2009).

[20] E. Ferrero, L. Foini, T. Giamarchi, A. Kolton, and A. Rosso, In preparation.